Overcoming limitations of nanomechanical resonators with simultaneous resonances

Najib Kacem, Sébastien Baguet, Laurent Duraffourg, G Jourdan, Régis Dufour, Sébastien Hentz

Overcoming limitations of nanomechanical resonators with simultaneous resonances

N. Kacem[1],* S. Baguet[4],† L. Duraffourg[2,3], G. Jourdan[2,3], R. Dufour[4], and S. Hentz[2,3‡]

[1]*FEMTO-ST Institute, UMR 6174, University of Franche Comté, UBFC, F-25000 Besançon, France*

[2]*Université Grenoble Alpes, F-38000 Grenoble, France*

[3]*CEA, LETI, Minatec Campus, F-38054 Grenoble, France*

[4]*Université de Lyon, CNRS INSA Lyon, LaMCoS UMR 5259, F-69621 Villeurbanne France*

Abstract

Dynamic stabilization by simultaneous primary and superharmonic resonances for high order nonlinearity cancellation is demonstrated with an electrostatically-actuated, piezoresistively-transduced nanomechanical resonator. We prove experimentally how the combination of both the third-order nonlinearity cancellation and simultaneous resonances can be used to linearly drive a nanocantilever up to very large amplitudes compared to fundamental limits like pull-in occurrence, opening the way towards resonators with high frequency stability for high-performance sensing or time reference.

PACS numbers: 85.85.+j, 05.45.-a, 46.40.Ff, 46.15.Ff

Nanoelectromechanical systems (NEMS) are being developed for many applications such as ultrasensitive mass[1–3] and gas sensing[4], subattonewton force detection at milliKelvin temperature[5] or single-spin detection[6]. Recently and due to the early occurrence of their nonlinearities[7], resonant nano-scale mechanical devices have been used as platforms to explore fundamental questions in nonlinear classical mechanics[8].

Large amplitude vibrations, while maintaining harmonic signals without distortion, are essential to the frequency stability of a resonator, and hence to the performance of a resonant nanosensor. The relative frequency noise spectral density of a resonator within its bandwidth is given by[9]:

$$S_f(\omega) = \left(\frac{1}{2Q}\right)^2 \frac{S_x(\omega)}{P_0} \tag{1}$$

where Q is the quality factor, S_x is the displacement spectral density and P_0 the displacement carrier power, *i.e.* the root mean square drive amplitude of the resonator $\frac{1}{2}A^2$.

The maximum amplitude is usually set by the onset of nonlinearity[10], either for stability reasons[11] or noise mixing in the carrier side bands[12]. Some work has been carried out in the past few years to overcome this limitation and stabilize the oscillation frequency of the resonator using an internal resonance that couples two different vibrational modes[13] or through hysteresis suppression by nonlinearity cancellation[7,10,14]. This is usually achieved by adding a negative contribution to the third order (Duffing) nonlinear term by means of an electrostatic gate for instance. Unfortunately, this technique is limited by higher order nonlinear terms which may be of importance even for small amplitudes, *i.e.* a fraction of the gap between the resonator and the electrode (typically below 20% of the actuation gap for electrostatically-actuated NEMS)[7]. The amplitude response can become a multivalued function of the frequency and five possible amplitudes for one given frequency is a clear signature of the physical significance of the fifth-order nonlinearities[15]. It has been shown how the use of simultaneous primary (drive force at ω_n, resonance at ω_n) and superharmonic (drive force at $\omega_n/2$, resonance at ω_n due to the second order nonlinear term) resonances can tune and dynamically delay the onset of this multivalued, highly unstable behavior[15].

In this paper, we demonstrate experimentally how the combination of these two techniques, namely the nonlinearity cancellation and simultaneous resonances, can be used to stabilize and drive a nanomechanical resonator almost linearly up to very large amplitudes compared to fundamental limits like pull-in occurrence.

The NEMS device (see Figs. 1(a) and 1(b)) consists of a cantilever beam of length $l = 5\,\mu m$, electrostatically driven and connected to two suspended piezoresistive gauges at a distance

$d = 0.15\,l$ from its anchored end. The cantilever vibration induces stress in the piezoresistive gauges which in turn is transduced into a resistance variation. It is fabricated on $200\,mm$ Silicon-On-Insulator wafers using complementary metal oxide semiconductor-compatible materials and processes. The readout scheme and process is fully detailed in[16].

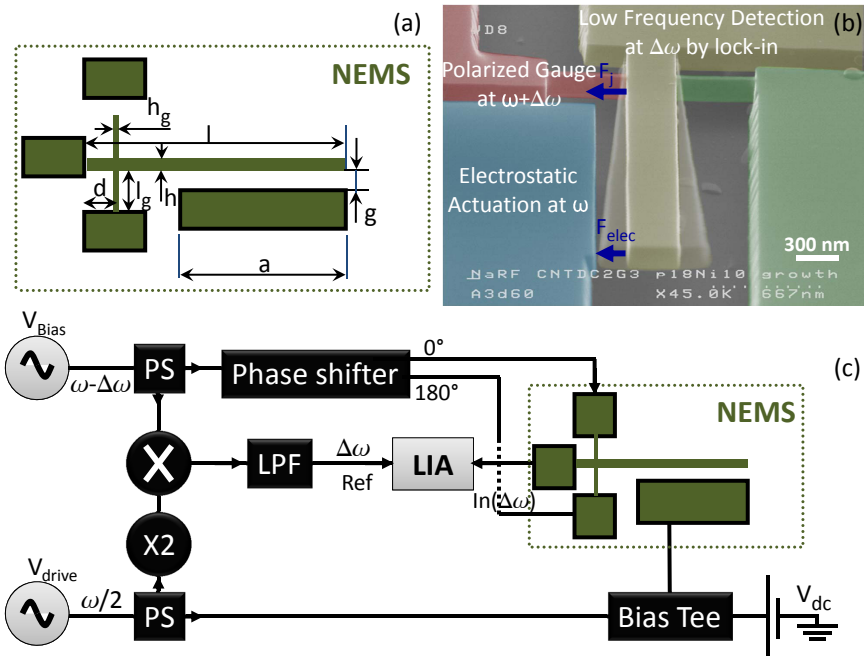

FIG. 1: (a): Design parameters of the NEMS device ($l = 5\,\mu m$, $a = 3.5\,\mu m$, $g = 200\,nm$, $d = 700\,nm$, $h = 300\,nm$, $l_g = 500\,nm$, $h_g = 80\,nm$). The gap g is the in plane distance between the cantilever and the electrode. (b): Food-coloured SEM image of the in-plane piezoresistive structure. (c): Electrical measurement scheme of the piezoresistive NEMS device for both 2Ω down mixing technique ($V_{dc} = 0$) and simultaneous resonances ($V_{dc} \neq 0$). V_{ac} and V_{dc} are respectively the alternating current (AC) and the direct current (DC) voltages applied to the drive electrode. V_b is the bias voltage applied to the nano-gauges, at a frequency slightly shifted from that of V_{ac} to down-mix the output voltage at a low frequency (typically a few 10kHz). LIA, PS and LPF are lock-in amplifier, power splitter and low pass filter, respectively.

The considered NEMS has shown excellent performance in terms of frequency stability, with more than $100\,dB$ dynamic range, and achievable mass resolution of few tens of zeptograms when operating in the linear domain[16,17]. We describe here how the electrostatic actuation of this nanoresonator is suitable to implement the simultaneous resonances and increase its dynamic range even further.

A variational approach, based on the extended Hamilton principle[18] has been used in order to derive the nonlinear equations of motion of the resonator in bending sketched in Figure 1(a). A reduced-order model is generated by modal decomposition transforming the continuous problem into a multi-degree-of-freedom system[10,14]. Assuming that the first mode is the dominant mode and neglecting the nonlinear damping, the resonator dynamics can be described by the following dimensionless nonlinear ordinary differential equation for a single degree-of-freedom a_1:

$$\begin{aligned} &\ddot{a_1} + \mu \dot{a_1} + \omega_n a_1 + \alpha_2 a_1^2 + \alpha_3 a_1^3 + \alpha_5 a_1^5 \\ &\quad = 4 V_{ac} V_{dc} \zeta \cos(\Omega t) + V_{ac}^2 \zeta \cos(2\Omega t) \end{aligned} \tag{2}$$

The dot denotes derivation with respect to time, ω_n the natural frequency, μ the constant damping coefficient, α_2, α_3, α_5, the coefficients of the quadratic, cubic and quintic nonlinearities respectively[7]. The amplitudes of the first and the second harmonic of the drive frequency Ω are respectively proportional to $V_{ac}V_{dc}$ and V_{ac}^2, where V_{ac} and V_{dc} are the AC and DC voltages applied to the nanoresonator and ζ is a constant that depends on the geometric parameters.

When Ω is tuned around $\frac{\omega_n}{2}$, the resonant response at ω_n is obtained by both the first and the second harmonic 2Ω. More precisely, the 2Ω-excitation mainly generates the primary resonance at ω_n, while due to nonlinearities, the Ω-excitation actuates a superharmonic resonance at ω_n. The response at ω_n is thus made of simultaneous primary and superharmonic resonances. The latter one is generated via a "slow" excitation compared to the resonant frequency. Experimentally, this can be achieved using the "2Ω mode" readout scheme described in Fig. 1(c). By contrast, if the frequency doubler is removed and the drive frequency is tuned around ω_n with $V_{dc} \neq 0$ and $V_{ac} \ll V_{dc}$, an "1Ω mode" is simply obtained for conventional primary resonance only.

The device under test was wire-bonded to a radio frequency (RF) circuit board and loaded in a vacuum chamber for measurements at room temperature. In order to avoid signal shortage by parasitic impedances, a down-mixing technique[19] was used to readout the resistance variation of the two nanowire gauges at a lower frequency $\Delta\omega$. Differential read-out was performed with in-phase and out-of-phase bias voltages V_b (one gauge is under compressive stress while the second one is under tensile stress)[16]. In order to analyze the dynamic behavior of the resonator under primary resonance and discuss the onset of nonlinearities, the conventional 1Ω mode (frequency doubler removed) was first used. The resonator was actuated using high DC voltages and a fixed AC bias voltage at the gauges ($V_b = 1.56\,V$ peak-to-peak) so as to reach the nonlinear regime. The frequency response was measured using a lock-in amplifier in frequency sweep-up and sweep-

down in order to obtain a full characterization of the resonator bifurcation topology. A constant quality factor $Q = 5000$ was measured on linear frequency resonance curves.

Figure 2 shows two nonlinear frequency responses in 1Ω mode. The right-hand-side resonance curve obtained for $V_{ac} = 150\,mV$ and $V_{dc} = 5\,V$ displays a hysteretic softening behavior characterized by an amplitude jump-up at the bifurcation point B_2 and an amplitude jump-down at the bifurcation point B_3 which is around 75% of the gap.

The response obtained for $V_{ac} = 75\,mV$ and $V_{dc} = 8\,V$ has a lower amplitude than the previous one because the actuation force is proportional to $V_{dc}.V_{ac}$ and has a direct consequence on the displacement amplitude. The DC voltage increase also affects the resonator stiffness *i.e.* shifts down the resonance frequency and amplifies the nonlinear electrostatic stiffness as well. Under those drive conditions, the mechanical Duffing nonlinearity is negligible with respect to the electrostatic one resulting in an amplified softening behavior (a stiffening behavior was also observed under different experimental conditions). Despite a lower amplitude, the influence of the high-order nonlinear terms and specifically of the quintic term ($\alpha_5 \propto V_{dc}^2$) is clearly visible: in frequency sweep-up, only one jump-up has been identified at the bifurcation point B_2. However, in frequency sweep-down, two jumps have been observed: a jump-up at the bifurcation point B_1 and a jump-down at the highest bifurcation point in the softening domain B_3 where the cantilever oscillation amplitude is around $52\,\%$ of the gap.

Obtaining a linear frequency response with this resonator at high amplitudes can be performed in principle under primary resonance only (1Ω mode) by cancelling out the cubic term ($\alpha_3(V_{dc}) = 0$) in Equation (2) and thus suppressing the hysteresis. α_3 depends on the mechanical and electrostatic parameters and in particular on the DC drive voltage. Assuming that the second harmonic in Equation (2) is negligible, the optimal DC drive voltage cancelling α_3 can be computed from[7]:

$$V_{dc_{OP}} = 3\frac{\sqrt{\sqrt{5.16 * g^{14}h^6 + \frac{10^4 g^{10}h^6}{(l-d)^{-4}}} - 4.53 g^7 h^3}}{10^{-9}(l-d)^4} \tag{3}$$

The mechanical displacement between the anchors and the gauges being negligible, the resonator is dynamically equivalent to a resonator of length $l - d$.

Applying Equation (3) to the resonator yields a relatively low optimal DC voltage $V_{dc_{OP}} \approx 1\,V$. Reaching large amplitudes (larger than the standard nonlinearity offset) in a linear fashion would then require significantly high AC voltages ($V_{ac} > 0.5\,V$). Consequently, the assumption of

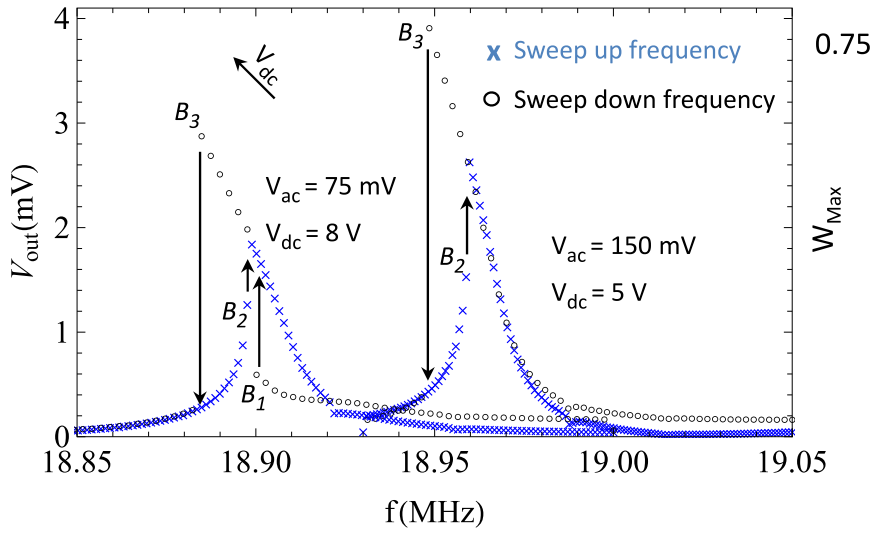

FIG. 2: Nonlinear resonance frequency responses measured using a 1Ω down-mixing technique and showing the location of the different bifurcation points $\{B_1, B_2$ and $B_3\}$. W_{max} is the nanoresonator displacement at its free end normalized by the gap. The hysteresis suppression is limited by high order nonlinear terms which leads to a highly unstable behavior for $V_{dc} = 8\,V$ and $V_{ac} = 75\,mV$.

negligible second harmonic terms is not valid anymore and Equation (3) is not applicable. More importantly, the non-linear terms of order five influence the dynamic behavior of the resonator already at low amplitudes as illustrated by the response ($V_{ac} = 75\,mV$, $V_{dc} = 8\,V$) plotted in Figure 2. The nonlinearity cancellation is thus limited by potential dynamic instability such as pull-in phenomena. Finally, no linear and stable behavior could be observed using the cancellation of the third-order terms with the resonator under primary resonance only.

In order to overcome this issue, we combined the use of this third-order term cancellation technique with the use of simultaneous primary and superharmonic resonances, which has been shown to delay the onset of the quintic non-linear terms[15]. In this case, Equation (2) can be solved using the method of multiple time scales and thus, the amplitude X and phase β modulations of the response can be written as:

$$\dot{X} = -\frac{\epsilon\left(20X\alpha_5\zeta_1^2\cos\beta + 9\alpha_2\omega_n^4\right)}{81\omega_n^9\left(4\zeta_1^2\sin\beta\right)^{-1}} - \frac{\epsilon\mu X}{2} + O(\varepsilon^2) \tag{4}$$

$$\dot{\beta} = -\frac{40\epsilon\alpha_5\zeta_1^4\{6+\cos(2\beta)\}}{81\omega_n^9} - \frac{6\epsilon\alpha_3X^2 + 5\epsilon\alpha_5X^4}{16\omega_n}$$
$$+2\sigma - \frac{2\epsilon\zeta_1^2\left(2\alpha_2\cos\beta + 6\alpha_3X + 15\alpha_5X^3\right)}{9\omega_n^5X} + O(\varepsilon^2) \tag{5}$$

where ε is the small nondimensional bookkeeping parameter and σ is the detuning parameter.

In Equations (4) and (5), both slow (superharmonic) and fast (primary) dynamics are present due to terms proportional to α_5 or α_2, the coefficients of the quintic and quadratic nonlinearities. The AC voltage sets the 2Ω excitation while the DC voltage only amplifies the Ω excitation. Unlike the case of primary resonance only shown in Figure 2, tuning the bifurcation topology in the present simultaneous resonances configuration can be obtained by simply increasing the DC voltage, i.e. amplifying the superharmonic excitation amplitude.

In practice, simultaneous primary and superharmonic resonances can be easily implemented with the 2Ω downmixing readout scheme described in Fig 1(c), with $V_{dc} \neq 0$. Moreover, high AC voltages should be used to increase the first harmonic $\cos(\Omega t)$ in Equation (2). The contribution of the AC voltage in the nonlinear electrostatic stiffness was taken into account in Equation (2) and the optimal drive DC voltage was analytically and numerically computed ($\alpha_3(V_{dc}, V_{ac}) = 0$) for $V_{ac} = 2V$, resulting in $V_{dc_{OP}} \approx 0.5\,V$. Fig. 3 shows a resonance peak obtained with these values. In this case, the resonator behavior is almost perfectly linear up to extremely high amplitudes compared to the actuation gap (above 95% of the gap) and only a slightly softening behavior remains. Computations predict that for this set of parameters the nonlinear electrostatic and mechanical stiffnesses are balanced and that the oscillation amplitude of the cantilever is close to $200\,nm$ at its free end (*i.e.* the width of the gap). The observed remaining softening part under these computed drive conditions are attributed to fabrication uncertainties and approximations in $V_{dc_{OP}}$ calculations.

In this experiment, the second-order nonlinear term α_2 giving rise to superharmonic resonance is used to control the stability of the nanoresonator around its primary resonance by retarding the effect of the fifth-order nonlinearity. The latter yields a highly unstable behavior with five possible amplitudes for one given frequency at amplitudes below 50% of the gap g as shown in Fig. 2. We demonstrate here how the use of simultaneous primary and superharmonic resonances permits the dynamic stabilization of the nonlinear nanoresonator in order to maintain a linear behavior at large-amplitude vibrations close to the gap. At this vibration level, the free end of the resonator reaches a distance of a few nm to the electrode without a damageable pull-in as would occur without the use of simultaneous resonance.

In order to experimentally confirm such an oscillation level, the DC voltage was gradually increased from $0.5\,V$ up to $2\,V$. Obviously, the vibration amplitude of the resonator should increase, eventually hitting the actuation electrode. Besides, the cantilever behavior should subsequently

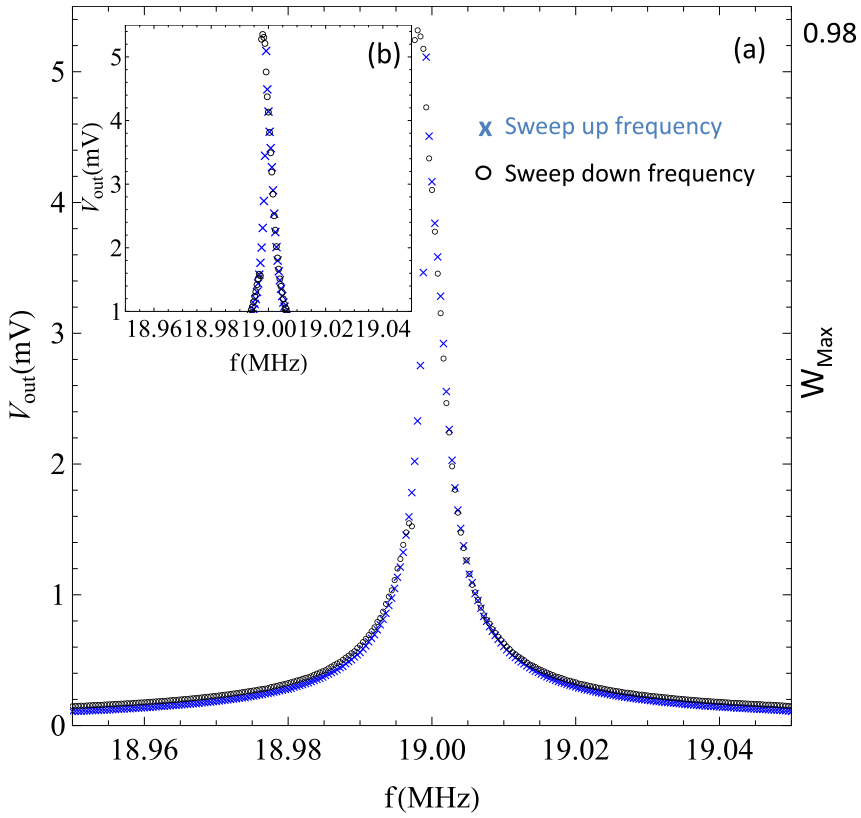

FIG. 3: (a): Slightly softening frequency response measured with the 2Ω down-mixing technique at the optimal DC voltage $V_{dc} = 0.5\,V$ for $V_{ac} = 2\,V$ ($V_b = 1.56\,V$). (b): Zoom in the frequency region of the resonance peak. Unlike the peaks obtained under primary excitation only in Figure 2, the combined use of third-order term cancellation with simultaneous primary and superharmonic resonances enable a stable and linear behavior of the nanomechanical resonator at very large amplitudes close to the actuation gap (the onset of unstability being here above $95\,\%$ of the gap g).

become more softening. Figure 4 shows the frequency response obtained for $V_{dc} = 2\,V$: the increase in the electrostatic softening nonlinear stiffness is evidenced by the frequency shift between the two bifurcation points (softening domain) which is significantly enlarged compared to Fig. 3. However the output signal at the peak is still $V_{out} \simeq 5.4mV$, *i.e.* the same value as at $V_{dc} = 0.5\,V$. The observed plateau is not due to any kind of electrical saturation and is very reproducible across multiple measurements. We attribute this to the fact that the resonator reached a stable vibration amplitude equal to the gap ($200\,nm$). At one given bias voltage, this can be interpreted as a measurement of the experimental output voltage sensitivity per unit of displacement of the cantilever free end and confirms the very high measured amplitude compared to the gap, see Fig. 3.

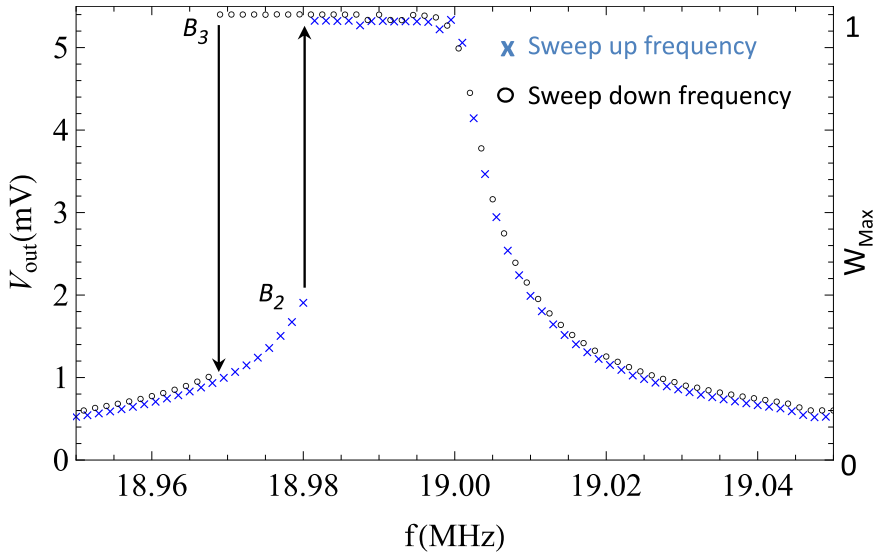

FIG. 4: Frequency response with $V_{dc} = V_{ac} = 2\,V$ ($V_b = 1.56\,V$). The horizontal branch intercepting the bifurcation point B_3 is not due to any saturation in the readout scheme. It rather shows that the cantilever free end comes in physical contact with the actuation electrode in a reproducible way. This further confirms the high vibration amplitude reached by the device in Fig. 3.

In this letter, a dynamic stabilization approach has been demonstrated on a nanomechanical resonator electrostatically actuated based on piezoresistive detection ($160\,nm$ thick) fabricated using a hybrid e-beam/deep ultraviolet lithography technique. The device has been characterized using a 1Ω down-mixing technique in its nonlinear regime to investigate the stability domain of the cantilever dynamics under primary resonance. It has been shown that the high-order nonlinearities limit drastically the operating domain of the nonlinearity cancellation. In order to overcome this limit, the sensor has been actuated under its primary and superharmonic resonances simultaneously by using a 2Ω readout scheme. Specifically, the bistability domain of the resonator can be significantly reduced and so it can operate almost linearly for displacements well beyond the multistability limit and almost up to the gap, while retarding undesirable behaviors and suppressing pull-in (of course, impact on surrounding elements is undesirable to avoid harmonic distortion).

This technique opens promising perspectives for time-reference or sensing purposes: the frequency stability of the device should be significantly improved compared to its operation in linear regime below the bistability limit. In particular, the mass resolution one can expect with this device without reaching any damaging amplitude and this technique is about 20 zeptograms (five times smaller than the performance reported in[16]). Specific devices will be fabricated in the near

future to substantiate this fact.

The authors are indebted to the Carnot Institutes Ingénierie@Lyon (I@L) and CEA LETI for their support and funding (NEMS Project).

---

* najib.kacem@femto-st.fr

† Sebastien.Baguet@insa-lyon.fr

‡ sebastien.hentz@cea.fr

[1] Y. T. Yang, C. Callegari, X. L. Feng, K. L. Ekinci, and M. L. Roukes, Nano Letters **6**, 583 (2006).

[2] K. Jensen, K. Kim, and A. Zettl, Nature Nanotechnology **3**, 533 (2008).

[3] V.-N. Nguyen, S. Baguet, C.-H. Lamarque, and R. Dufour, Nonlinear Dynamics **79**, 647 (2015).

[4] X. M. H. Huang, M. Manolidis, S. C. Jun, and J. Hone, Applied Physics Letters **86**, 143104 (2005).

[5] H. J. Mamin and D. Rugar, Applied Physics Letters **79**, 3358 (2001).

[6] D. Rugar, R. Budakian, H. J. Mamin, and B. W. Chui, Nature **430**, 329 (2004).

[7] N. Kacem, J. Arcamone, F. Perez-Murano, and S. Hentz, Journal of Micromechanics and Microengineering **20**, 045023 (2010).

[8] R. Lifshitz and M. Cross, "Nonlinear dynamics of nanomechanical resonators," in *Nonlinear Dynamics of Nanosystems* (Wiley-VCH Verlag GmbH & Co. KGaA, 2010) pp. 221–266.

[9] W. P. Robins, *Phase Noise in Signal Sources* (Institution of Engineering and Technology, 1984).

[10] I. Kozinsky, H. W. C. Postma, I. Bargatin, and M. L. Roukes, Applied Physics Letters **88**, 253101 (2006).

[11] B. Yurke, D. S. Greywall, A. N. Pargellis, and P. A. Busch, Phys. Rev. A **51**, 4211 (1995).

[12] V. Kaajakari, J. Koskinen, and T. Mattila, Ultrasonics, Ferroelectrics and Frequency Control, IEEE Transactions on **52**, 2322 (2005).

[13] D. Antonio, D. H. Zanette, and D. López, Nature communications **3**, 806 (2012).

[14] L. C. Shao, M. Palaniapan, and W. W. Tan, Journal of Micromechanics and Microengineering **18**, 065014 (2008).

[15] N. Kacem, S. Baguet, R. Dufour, and S. Hentz, Applied Physics Letters **98**, 193507 (2011).

[16] E. Mile, G. Jourdan, I. Bargatin, S. Labarthe, C. Marcoux, P. Andreucci, S. Hentz, C. Kharrat, E. Colinet, and L. Duraffourg, Nanotechnology **21**, 165504 (2010).

[17] M. S. Hanay, S. Kelber, A. K. Naik, D. Chi, S. Hentz, E. C. Bullard, E. Colinet, L. Duraffourg, and

M. L. Roukes, Nature Nanotechnology **7**, 602 (2012).

[18] A. H. Nayfeh and M. I. Younis, Journal of Micromechanics and Microengineering **15**, 1840 (2005).

[19] I. Bargatin, E. B. Myers, J. Arlett, B. Gudlewski, and M. L. Roukes, Applied Physics Letters **86**, 133109 (2005).